Application of virtual screening to the discovery of novel nicotinamide phosphoribosyltransferase (NAMPT) inhibitors with potential for the treatment of cancer and axonopathies

David E. Clark [a],*, Bohdan Waszkowycz [a],†, Melanie Wong [a], Peter M. Lockey [a], Robert Adalbert [c],‡, Jonathan Gilley [c],‡, Jonathan Clark [b], Michael P. Coleman [c],‡

[a] Charles River Laboratories, 8/9 Spire Green Centre, Flex Meadow, Harlow, Essex CM19 5TR, United Kingdom
[b] Babraham Bioscience Technologies Ltd, Babraham Research Campus, Cambridge CB22 3AT, United Kingdom
[c] The Babraham Institute, Babraham Research Campus, Babraham, Cambridge CB22 3AT, United Kingdom

ARTICLE INFO

ABSTRACT

NAMPT may represent a novel target for drug discovery in various therapeutic areas, including oncology and inflammation. Additionally, recent work has suggested that targeting NAMPT has potential in treating axon degeneration. In this work, publicly available X-ray co-crystal structures of NAMPT and the structures of two known NAMPT inhibitors were used as the basis for a structure- and ligand-based virtual screening campaign. From this, two novel series of NAMPT inhibitors were identified, one of which showed a statistically significant protective effect when tested in a cellular model of axon degeneration.
© 2016 The Authors. Published by Elsevier Ltd. This is an open access article under the CC BY-NC-ND license (http://creativecommons.org/licenses/by-nc-nd/4.0/).

Previously identified as a cytokine (pre-B-cell colony enhancing factor, PBEF) and also claimed as an insulin-mimetic hormone (visfatin), nicotinamide phosphoribosyltransferase (NAMPT) converts nicotinamide to nicotinamide mononucleotide (NMN), which is a key nicotinamide adenine dinucleotide (NAD) intermediate. NAMPT is currently of much interest in a number of fields of research, including NAD biology, metabolism and inflammation.[1,2] NAMPT activity has been shown to be essential for maintaining adequate intracellular NAD levels, suggesting that it may play a central role in modulating the activity of a wide range of NAD-dependent enzymes. By regulating NAD availability, NAMPT is able to control both cell viability and the inflammatory response. For instance, tumor cells develop dependence on NAMPT due to their increased energy requirements and the elevated activity of NAD-consuming enzymes such as the sirtuins and poly(ADP-ribose) polymerases.[3] NAMPT may thus represent a novel target for drug discovery in various therapeutic areas, including oncology and inflammation[2,4] and, as a consequence, there has been a great deal of research effort by the medicinal chemistry community seeking novel inhibitors of the target.[5]
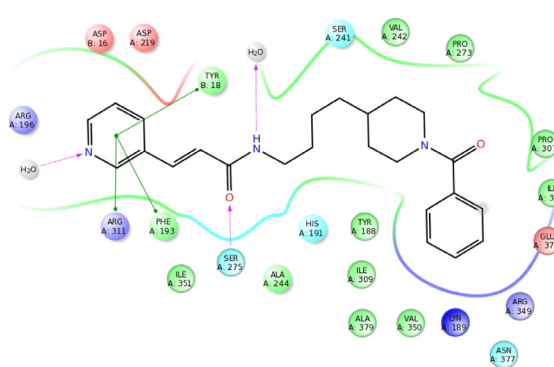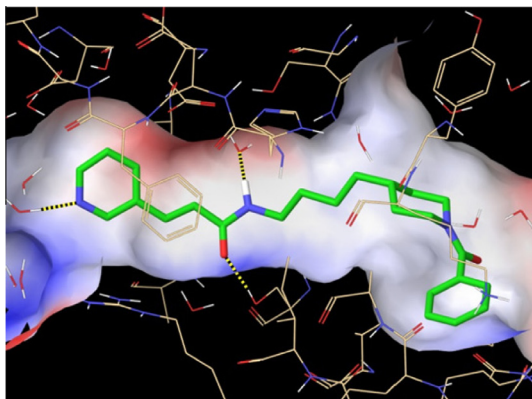
In addition, recent work has suggested that targeting NAMPT may also be beneficial in treating axon degeneration.[6] The subsequent enzyme in the NAD salvage pathway, NMNAT, greatly delays axon degeneration in injury and some disease models when a stable isoform is targeted to axons.[7–9] Axon degeneration is an early feature of many neurodegenerative diseases and needs to be prevented for treatments to be effective. NAMPT inhibitors FK866 and CHS828 both phenocopy the protective effect of NMNAT when applied at the time of, or subsequent to, axonal transection.[6,10,11] This suggests that accumulation of the NMNAT substrate (and NAMPT product) NMN within axons is at least partly responsible for their degeneration after endogenous axonal NMNAT is degraded, potentially in addition to depletion of axonal NAD. As many established cancer chemotherapeutics are toxic to axons,[12] NAMPT inhibition offers the attractive possibility of contributing to cancer treatment while simultaneously preserving axons during a regime of chemotherapy. Here, we report the identification of novel, small molecule inhibitors of NAMPT for axonopathies, and potentially other indications, by means of a virtual screening campaign using structure- and ligand-based techniques.

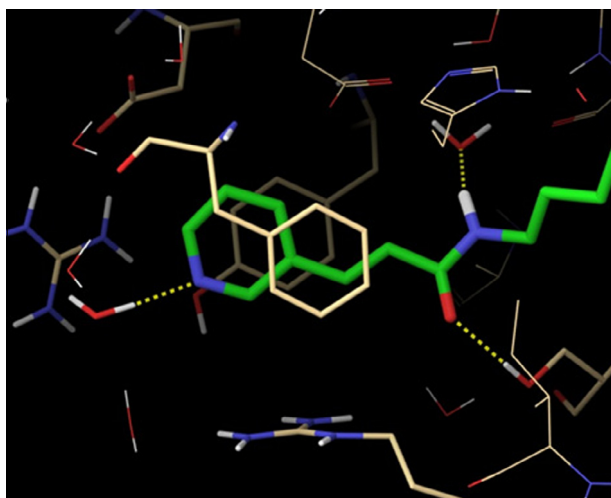* Corresponding author. Tel.: +44 (0) 1279 645 611; fax: +44 (0) 1279 645 646.
E-mail address: david.clark@crl.com (D.E. Clark).
† Current address: Drug Discovery Unit, Cancer Research UK Manchester Institute, The University of Manchester, Wilmslow Road, Manchester M20 4BX, United Kingdom.
‡ Current address: John van Geest Centre for Brain Repair, Department of Clinical Neurosciences, University of Cambridge, Robinson Way, Cambridge CB2 0PY, United Kingdom.
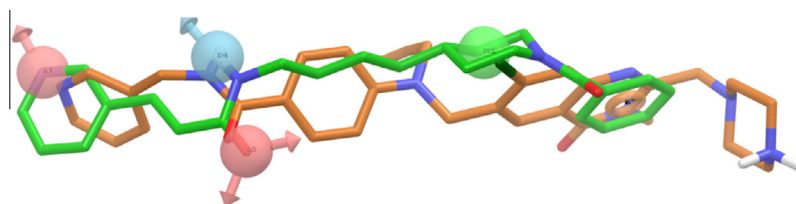
Figure 1. X-ray structure (left) and schematic ligand interaction diagram (right) of FK866 bound to NAMPT showing water molecules that mediate contacts between the ligand and protein.

Figure 2. Details of the binding interactions of FK866 in PDB structure 2GVJ showing the aromatic stacking (Phe193, Tyr18B) around the pyridine-vinyl head group.

Table 1
Chemical structures of known NAMPT inhibitors used as queries for ligand-based virtual screening
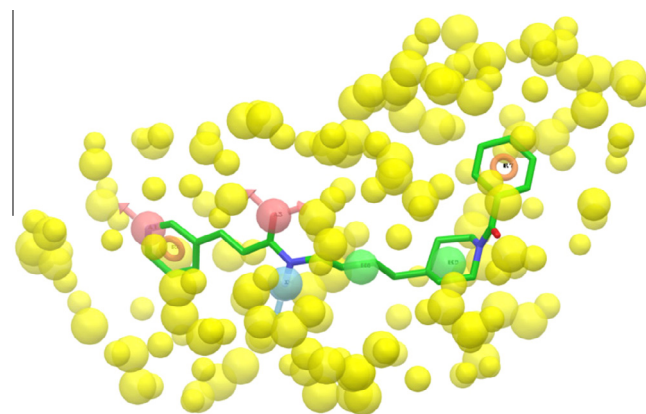
Compound	Structure
1	
2	

The structure-based virtual screen (SBVS) employed the publicly available X-ray crystal structures of NAMPT in complex with FK866 (PDB code: 2GVJ) and nicotinamide mononucleotide (NMN, PDB code: 2GVG). The binding interactions of FK866 are depicted in Figure 1.

Although FK866 occupies a relatively extended binding site, there is only one direct hydrogen bond to the enzyme (to Ser275) and two water-mediated hydrogen bonds (to Asp219 and Wat242 via Wat645). The X-ray structure also shows a water molecule within hydrogen-bonding distance of the pyridine group. Figure 2 shows in more detail the close aromatic stacking of the pyridine-vinyl head group between Phe193 and Tyr18B. In contrast, the benzoyl-piperidine tail is more loosely bound, with the phenyl ring occupying a small pocket bounded by the side chains of Lys189 and Arg349.

The Glide program[13] was used to dock various datasets of commercially available compounds into the active site of NAMPT. These compound sets had been pre-filtered using molecular property (e.g., $250 \leqslant MW \leqslant 450$, $-0.5 \leqslant C\log P \leqslant 4.0$ and

Figure 4. The E-pharmacophore query generated from the 2GVJ X-ray structure. Excluded volumes are shown in yellow.

Figure 3. The five-point common pharmacophore query derived from FK866 (green carbon atoms) and MPI-0479626 (orange carbon atoms).

Table 2
Summary of ligand-based virtual screening results

Search type	Number of hits selected
2D substructure	94
2D similarity	79
3D pharmacophore	95
3D similarity	153
E-pharmacophore	72

Table 3
Breakdown of activities for the 40 compounds for which IC_{50} values were determined

Activity range	Number of compounds
100 nM $\leqslant IC_{50} < 1$ μM	5
1 μM $\leqslant IC_{50} < 10$ μM	15
$IC_{50} \geqslant 10$ μM	20

TPSA $\leqslant 120$ Å^2) and substructural criteria[14] to remove non-drug-like molecules. In the interests of generating the most diverse results possible in a timely manner, it was decided to run the following docking screens:

- *SBVS1*—as the most conservative approach to finding close analogues of FK866, a 46,000-compound dataset of *meta*-pyridine-containing structures was docked against the 2GVJ structure including both Wat645 and Wat1339; the latter water helps compounds to achieve an FK866-like binding of the pyridine group;
- *SBVS2*—as a more open-ended screen, a larger, more diverse dataset of 750,000 compounds was docked to the 2GVJ structure including only Wat645. Removal of Wat1339 enables more diverse chemotypes to bind to the pyridine subsite;
- *SBVS3*—to encourage more diversity in ligand binding, the larger dataset was docked to the 2GVG structure containing no waters. Although 2GVG is very similar to 2GVJ, small changes in amino acid side chain positions can sometimes influence the docking results and yield different solutions. Removal of Wat645 also allows for larger amide mimics to bridge between Ser275 and Asp219.

For *SBVS1*, the Glide SP protocol was used to dock the *meta*-pyridine dataset, constraining at least one hydrogen bond to either Ser275 or Wat645, on the basis that compounds forming neither

Table 4
Chemical structures, IC_{50} values and provenance for selected hits identified by the first round of virtual screening

Compound	Structure	NAMPT IC_{50} (μM)	Provenance
3		0.22	SBVS
4		0.32	LBVS
5		0.67	SBVS
6		0.78	LBVS
7		0.94	LBVS
8		1.9	LBVS
9		3.2	LBVS
10		3.8	SBVS
11		5.0	LBVS

of the amide hydrogen bonds would not be very plausible ligands. For *SBVS2* and *SBVS3*, the 750K-compound dataset was too large for docking with Glide SP in a reasonable timeframe. Therefore, the dataset was docked with the faster Glide HTVS protocol and the top-scoring 50,000 solutions were re-docked using Glide SP. Hydrogen bond constraints to Ser275 or Wat645 (if present) were added as before. Default Glide docking parameters were applied, with the post-docking geometry minimization stage (and incorporation of estimated strain energy into the docking score) included for the Glide SP jobs. One pose per input ligand was retained, and a maximum of 30,000 solutions per SP docking run retained for analysis.

The analysis of the docked compounds from each of the docking screens involved using the Maestro graphical interface to search for compounds of interest based on a combination of binding features and docking score, and manual visualization of sets of a few thousand docked ligands. Analysis was further facilitated by partitioning the ligands into molecular weight bins, so that a balanced selection could be made across different molecular weight ranges. The analysis resulted in a set of 630 compounds for consideration (221 from *SBVS1*, 276 from *SBVS2*, and 133 from *SBVS3*).
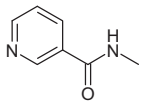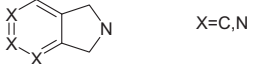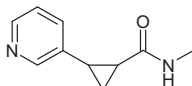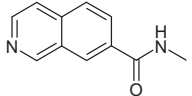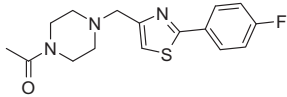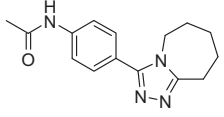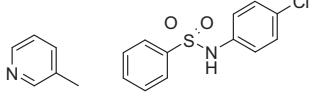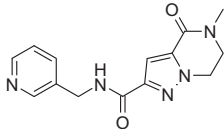
As a complement to the structure-based campaign described above, a ligand-based strategy was also pursued. An assessment of the known ligands for NAMPT suggested that the compounds fell into two broad classes: those with long aliphatic linkers and those with a phenyl ring in the linker. It was decided to carry out ligand-based virtual screening (LBVS) with a representative of each of these classes and so MPI-0479626[3] (**1**) and FK866 (**2**) (Table 1) were selected as query ligands.

Multiple 2D and 3D ligand-based searches were undertaken using these query compounds. The 2D searches utilized a database of 2.35 million commercially available compounds while the 3D searches were run against the 750,000-compound database mentioned earlier. In brief, the following searches were carried out:

- *2D substructure*—given the presence of a terminal *meta*-pyridine in both query ligands plus a knowledge of this moiety's binding mode in the NAMPT active site, it was decided to search for compounds that possessed this group connected by a two-atom linker to a carbonyl group. These searches were carried out using Daylight[15] SMARTS queries.
- *2D fingerprint*—several similarity searches were carried out around the two compounds using Daylight[15] fingerprints and 12 different fingerprint types available within Canvas.[16]
- *3D pharmacophore*—3D pharmacophores were derived and searched for using Phase.[17] Query pharmacophores were based on the individual compounds and an additional common pharmacophore was derived (Fig. 3).
- *3D shape similarity*—Phase Shape[18] was used to carry out 3D similarity searches based on the two query ligands. Initial experiments with FK866 revealed that it was difficult to find good matches to the whole ligand and particularly for the key terminal pyridine moiety. Therefore, the search database was changed to use just a focused set of ~8000 terminal *meta*-pyridines identified in the 2D substructure searches mentioned above.
- *E-pharmacophore*—this method[19] combines pharmacophore perception with protein–ligand energetic terms computed by the Glide XP scoring function to rank the importance of pharmacophore features. It was applied to the FK866:NAMPT co-crystal structure (2GVJ). The result was a seven-feature pharmacophore together with a set of excluded volume spheres denoting the steric boundaries of the NAMPT active site (Fig. 4).

The results of all the ligand-based searches are summarized in Table 2. Overall, 493 compounds were selected from all the

Table 5
2D substructural queries used for follow-up searches

2D substructure query	Purpose
	Search for a linker not seen in round 1 hits. In this and other queries containing a pyridine ring, no substitution was permitted on the pyridine ring
X=C,N	Search for a novel head-group and/or linker. In these searches, the atoms marked 'X' were allowed to be either carbon or nitrogen
	Search for novel linker
	Search for novel head-group
	Search for other compounds containing this tail-group (from compound **9**) but with other head-groups
	Search for other compounds containing this tail-group (from compound **5**) but with other head-groups
	This query used the Daylight SMARTS '.' convention to specify that a biaryl sulfonamide (as seen in compound **8**) should be present in addition to a *meta*-substituted pyridine, but did not specify how the two moieties should be linked. In the biaryl fragment part of the query, all the aromatic atoms were set to atom type 'a' to allow them to match any aromatic atom
	Search for other compounds containing this fragment (observed in compound **4**) which lacks the unwanted alpha–beta unsaturated carbonyl in the linker

Table 6
Breakdown of activities for the 41 compounds for which IC$_{50}$ values were determined
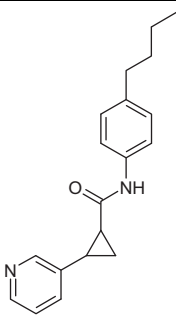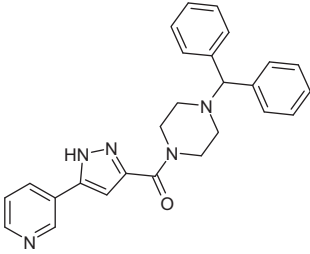
Activity range	Number of compounds
IC$_{50}$ < 100 nM	4
100 nM $\leqslant$ IC$_{50}$ < 1 µM	9
1 µM $\leqslant$ IC$_{50}$ < 10 µM	8
IC$_{50}$ $\geqslant$ 10 µM	20

searches. When duplicates were removed from this list, a final set of 417 unique compounds remained.

Combining the 630 unique hits obtained from the structure-based virtual screening with the 417 from the ligand-based campaign gave a total of 1047 compounds. When duplicates were removed, 1028 compounds remained, indicating a very small overlap between the hits selected by the two types of virtual screen. This set of 1028 compounds represents a diverse collection of potential NAMPT inhibitors. This fact was demonstrated by clustering the set (using Daylight[15] fingerprints, Ward's clustering method[20] and a Tanimoto similarity threshold of 0.85), an operation that resulted in 878 clusters.

After review by a medicinal chemist taking into account (subjective) criteria such as chemical tractability and apparent

Table 7
Chemical structures, IC$_{50}$ values and key calculated properties for the most potent examples of the two series identified by the second round of virtual screening

Compound	Series	Structure	IC$_{50}$ (nM)	MW, TPSA (Å^2), $C\log P$, LE, LLE
12	Cyclopropyl		41.8	294.4, 42.0, 3.85, 0.46, 3.49
13	Pyrazole		242.7	423.5, 65.1, 3.15, 0.28, 2.79

Compound **12** is assumed to be a mixture of four stereoisomers. Physicochemical properties were calculated using Advanced Chemistry Development, Inc.'s Percepta program.[22]

Table 8
Plasma protein binding and CYP inhibition data

Compound number	Human plasma protein binding (% bound)	CYP1A2% inhib. @ 3 μM	CYP2C9% Inhib. @ 3 μM	CYP2D6% Inhib. @ 3 μM	CYP3A4% Inhib. @ 3 μM
12	99.2	22	31	1	63
13	99.6	23	43	3	20

similarities to and differences from known NAMPT inhibitors, it was decided to order 102 compounds from the appropriate commercial vendors. 99 of the 102 compounds were received and of these, 42 showed 50% inhibition or greater when screened in the primary assay[21] at 100 μM in singlet. 40 compounds were confirmed to be hits when retested in duplicate at 100 μM and IC$_{50}$ values were determined for these. A breakdown of the distribution of the resulting IC$_{50}$ values is shown in Table 3.

The five sub-micromolar compounds are shown in Table 4, along with some other compounds in the single-digit micromolar range that contain potentially novel structural features in the context of NAMPT inhibitors, e.g., in terms of the nature of the linker moiety to the terminal *meta*-pyridine. It is noteworthy that both structure- and ligand-based techniques contributed to this set of hits underlining the value of carrying out both types of search.

In a second round of virtual screening, multiple 2D substructure and similarity searches were carried out seeking, in particular, analogues lacking the potentially problematic alpha–beta unsaturated

carbonyl group. Specifically, 2D similarity searches were carried out using hit compounds **3**, **4**, **10** and **11** as queries and a set of eight 2D substructure searches using the queries shown in Table 5. These queries were intended to follow-up on interesting structural features observed in the first round hits and to try to find alternatives to the *meta*-pyridine as well as additional linker groups. All searches were carried out using the previously mentioned database of 2.35 million commercially available compounds.

This effort led to the purchase and testing of an additional 79 compounds. 41 of these went on to have IC$_{50}$ values determined. A breakdown of the activities of these 41 compounds is provided in Table 6. The most active compound discovered in this second round of screening showed an IC$_{50}$ value of 41.8 nM.
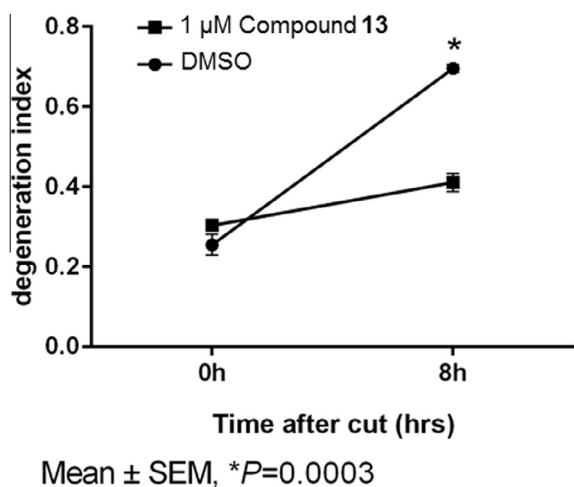
Reviewing these results led to the identification of two distinct series both lacking the alpha–beta unsaturated carbonyl group. The most active example of each series is shown in Table 6 along with some key calculated properties. Fresh solid samples of the two compounds were obtained and submitted for analytical testing (LC/MS and NMR). For both compounds, the observed ^{1}H NMR spectrum was consistent with the structure shown in Table 7 and the purities were acceptable (93% and 99% for **12** and **13**, respectively).

The two heads of series were also profiled in a panel of in vitro ADME assays to identify liabilities that would need to be addressed during hit-to-lead optimization. The results of these tests are shown in Tables 8 and 9.

The data show that both compounds are highly protein bound and there are potential CYP450 liabilities that would need to be dealt with during hit-to-lead optimization. Compound **13** shows

Table 9
Microsomal stability and Caco-2 permeability data. Microsomal stability data reflect% of parent compound remaining at 30 min, with the compounds being tested at 5 μM

Compound number	Microsomal stability (human, + NADPH)	Microsomal stability (human, − NADPH)	Microsomal stability (mouse, + NADPH)	Microsomal stability (mouse, − NADPH)	Caco-2 permeability × 10^{-6} cm/s
12	7	96	43	87	<70% recovery
13	63	104	19	96	<70% recovery

Figure 5. Compound **13** delays degeneration of injured axons in a cellular assay.

cervical ganglion explant cultures from neonatal mice were treated with each test compound less than 10 min before axons were transected using a microscalpel. Images were captured by phase contrast microscopy and degeneration index calculated as previously described.[6] Compound **13** administered at 1 μM protected injured axons significantly at 8 h after cut (Fig. 5).

Figure 6 shows a comparison of the effect on transected axons of 100 nM FK866 and 1 μM **13** with a control (DMSO). Qualitatively, it can be seen that the DMSO treated axons degenerate faster over time than axons treated with either of the compounds. While the protection afforded by **13** in this assay was less prolonged than that obtained with the more potent FK866,[6] this result is nonetheless encouraging for an unoptimised compound and demonstrates the effectiveness of our virtual screening strategy in identifying molecules with the desired biological effect.

At the time this work was completed (late 2012), to the best of our knowledge neither of the chemotypes discovered had been reported in the context of NAMPT inhibition. More recently, Genentech and Forma have published a paper[23] describing cyclopropyl-linked NAMPT inhibitors discovered using fragment-based screening. The highlighted example from the publication is shown in Table 10 with associated in vitro biochemical data. Following in vitro ADME profiling, compound **14** was orally dosed to nude mice (10 mg/kg b.i.d.) and displayed good plasma exposures over a 24 h period with free concentrations constantly exceeding the cellular anti-proliferation IC_{50} values. Subsequently, the compound also showed strong efficacy in an HT-1080 fibrosarcoma xenograft model when orally administered for five days to tumor-bearing
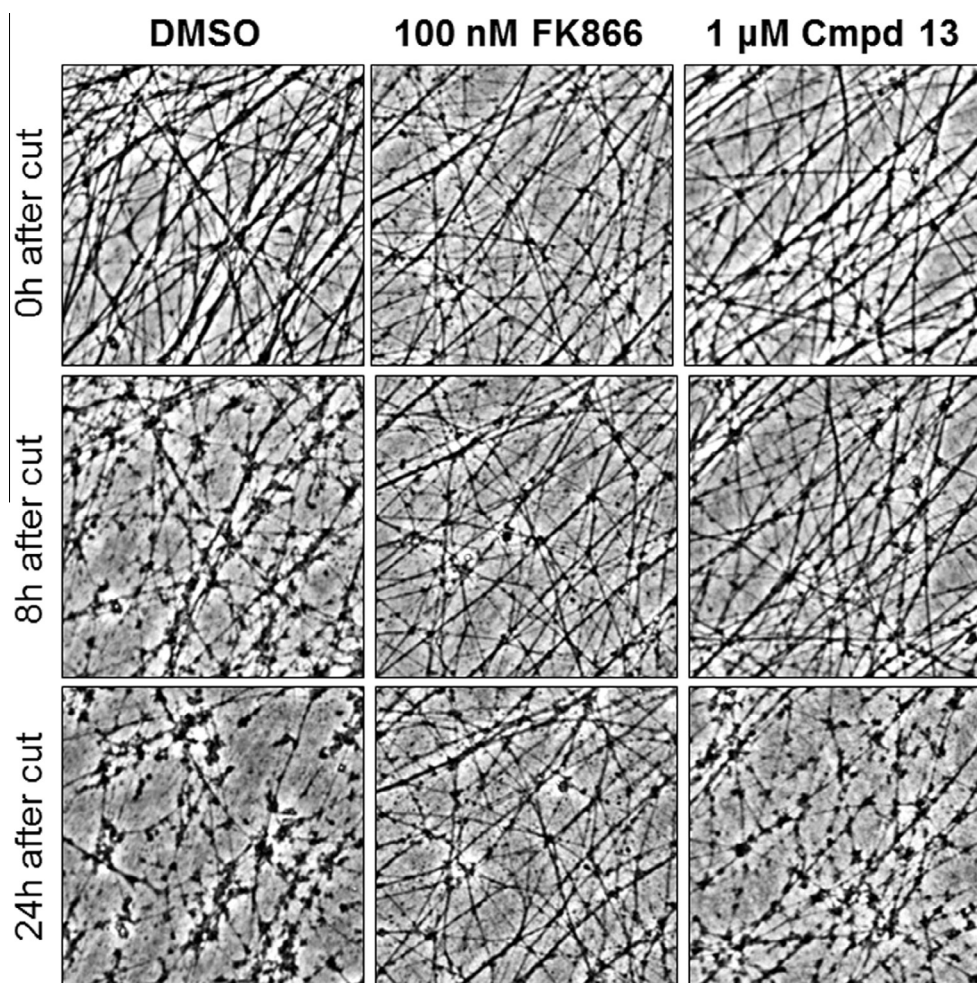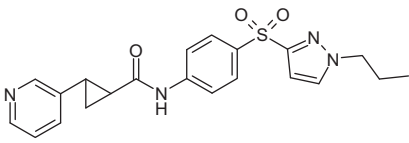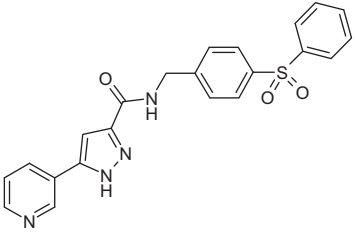
moderate stability in the presence of human and mouse liver microsomes (with co-factor) but **12** appears particularly vulnerable to metabolism by human microsomes. In terms of Caco-2 permeability, the results for both compounds were affected by low recovery, but the experiments (and in silico calculations[22]) suggested that the compounds would be highly permeable.

A cellular assay for axon survival was established and used to test the two heads of series (compounds **12** and **13**). Superior

Figure 6. Comparison of DMSO-treated (control) axons with those treated with 100 nM FK866 and 1 μM of compound **13** at time of cut, and 8 h and 24 h post-cut.

Table 10
Example compounds from Refs. 16,17 having similar structures to the series discovered in this work

Compound number	Structure	NAMPT IC$_{50}$ (nM)	Cellular IC$_{50}$ (nM)
14		5.1	1.3 ± 0.2 (HT-1080)
15		43	>10,000 (A2780)

nude mice using the same dosing regimen. Furthermore, the observed anti-tumor effects were achieved with minimal impact on the mouse body weights.[23] Coincidentally, the same companies also published a compound similar to our pyrazole-linked example in a slightly earlier (but still post-2012) paper[24] (**15**, Table 10) describing a structure-based design approach to NAMPT inhibitor discovery. Interestingly, the sulfone element in both compounds is reminiscent of the sulfonamide seen in **8** (Table 4).

In conclusion, we have described a structure- and ligand-based virtual screen that resulted in the rapid and cost-effective discovery of two series of NAMPT inhibitors that were novel in that context at the time of their discovery and had good potential for further optimization (although, for commercial reasons, this was never pursued). The subsequent publications from other groups reporting similar compounds bears out the effectiveness of the strategy employed. Encouragingly, one of the hits from the virtual screen showed a statistically significant protective effect when tested in a cellular model of axon degeneration adding weight to the hypothesis[6] that small molecule inhibition of NAMPT may be a fruitful approach to the treatment of neurodegenerative diseases.

References and notes

1. Garten, A.; Schuster, S.; Penke, M.; Gorski, T.; de Giorgis, T.; Kiess, W. *Nat. Rev. Endocrinol.* **2015**, *11*, 535.
2. Montecucco, F.; Cea, M.; Cagnetta, A.; Damonte, P.; Nahimana, A.; Ballestrero, A.; Del Rio, A.; Bruzzone, S.; Nencioni, A. *Curr. Top. Med. Chem.* **2013**, *13*, 2930.
3. Fleischer, T. C.; Murphy, B. R.; Flick, J. S.; Terry-Lorenzo, R. T.; Gao, Z.-H.; Davis, T.; McKinnon, R.; Ostanin, K.; Willardsen, J. A.; Boniface, J. J. *Chem. Biol.* **2010**, *17*, 659.
4. Sampath, D.; Zabka, T. S.; Misner, D. L.; O'Brien, T.; Dragovich, P. S. *Pharmacol. Ther.* **2015**, *151*, 16.
5. Galli, U.; Travelli, C.; Massarotti, A.; Fakhfouri, G.; Rahimian, R.; Tron, G. C.; Genazzani, A. A. *J. Med. Chem.* **2013**, *56*, 6279.
6. Di Stefano, M.; Nascimento-Ferreira, I.; Orsomando, G.; Mori, V.; Gilley, J.; Brown, R.; Janeckova, L.; Vargas, M. E.; Worrell, L. A.; Loreto, A., et al. *Cell Death Differ.* **2015**, *22*, 731.
7. Mack, T. G.; Reiner, M.; Beirowski, B.; Mi, W.; Emanuelli, M.; Wagner, D.; Thomson, D.; Gillingwater, T.; Court, F.; Conforti, L.; Fernando, F. S.; Tarlton, A.; Andressen, C.; Addicks, K.; Magni, G.; Ribchester, R. R.; Perry, V. H.; Coleman, M. P. *Nat. Neurosci.* **2001**, *4*, 1199.
8. Gilley, J.; Coleman, M. P. *PLoS Biol.* **2010**, *8*, e1000300.
9. Conforti, L.; Gilley, J.; Coleman, M. P. *Nat. Rev. Neurosci.* **2014**, *15*, 394.
10. Sasaki, Y.; Vohra, B. P.; Lund, F. E.; Milbrandt, J. *J. Neurosci.* **2009**, *29*, 5525.
11. Loreto, A.; Di Stefano, M.; Gering, M.; Conforti, L. *Cell Rep.* **2015**, *13*, 2539–2552.
12. Cashman, C. R.; Höke, A. *Neurosci. Lett.* **2015**, 596.
13. (a) Friesner, R. A.; Murphy, R. B.; Repasky, M. P.; Frye, L. L.; Greenwood, J. R.; Halgren, T. A.; Sanschagrin, P. C.; Mainz, D. T. *J. Med. Chem.* **2006**, *49*, 6177; (b) Halgren, T. A.; Murphy, R. B.; Friesner, R. A.; Beard, H. S.; Frye, L. L.; Pollard, W. T.; Banks, J. L. *J. Med. Chem.* **2004**, *47*, 1750; (c) Friesner, R. A.; Banks, J. L.; Murphy, R. B.; Halgren, T. A.; Klicic, J. J.; Mainz, D. T.; Repasky, M. P.; Knoll, E. H.; Shaw, D. E.; Shelley, M.; Perry, J. K.; Francis, P.; Shenkin, P. S. *J. Med. Chem.* **2004**, *47*, 1739.
14. (a) Hann, M.; Hudson, B.; Lewell, X.; Lifely, R.; Miller, L.; Ramsden, N. *J. Chem. Inf. Comput. Sci.* **1999**, *39*, 897; (b) Pearce, B. C.; Sofia, M. J.; Good, A. C.; Drexler, D. M.; Stock, D. A. *J. Chem. Inf. Model.* **2006**, *1060*, 46; (c) Baell, J. B.; Holloway, G. A. *J. Med. Chem.* **2010**, *53*, 2719.
15. Daylight Chemical Information Systems, Inc., PO Box 7737, Laguna Niguel, CA 92677, USA, http://www.daylight.com.
16. (a) Duan, J.; Dixon, S. L.; Lowrie, J. F.; Sherman, W. *J. Mol. Graphics Model.* **2010**, *29*, 157; (b) Sastry, M.; Lowrie, J. F.; Dixon, S. L.; Sherman, W. *J. Chem. Inf. Model.* **2010**, *50*, 771.
17. (a) Dixon, S. L.; Smondyrev, A. M.; Knoll, E. H.; Rao, S. N.; Shaw, D. E.; Friesner, R. A. *J. Comput. Aided Mol. Des.* **2006**, *20*, 647; (b) Dixon, S. L.; Smondyrev, A. M.; Rao, S. N. *Chem. Biol. Drug Des.* **2006**, *67*, 370.
18. Sastry, G. M.; Dixon, S. L.; Sherman, W. *J. Chem. Inf. Model.* **2011**, *51*, 2455.
19. (a) Salam, N. K.; Nuti, R.; Sherman, W. *J. Chem. Inf. Model.* **2009**, *49*, 2356; (b) Loving, K.; Salam, N. K.; Sherman, W. *J. Comput. Aided Mol. Des.* **2009**, *23*, 541.
20. Ward, J. H. *J. Am. Stat. Assoc.* **1963**, *58*, 236.
21. (a) Formentini, L.; Moroni, F.; Chiarugi, A. *Biochem. Pharmacol.* **2009**, *77*, 1612; (b) Zhang, R. Y.; Qin, Y.; Lu, X. Q.; Wang, P.; Xu, T. Y.; Zhang, L.; Miao, C. Y. *Anal. Biochem.* **2011**, *412*, 18. A fluorometric NAMPT assay was established based on these two publications in 96-well microplate format using commercially available NAMPT enzyme from Cyclex. Enzyme and substrate concentration, incubation time, temperature, and DMSO tolerance were investigated and optimised. The assay was validated using the standard inhibitors CHS-828 and FK866. The reproducibility of the assay was good with Z' values of greater than 0.7 and a % CV across the plate of less than 4%.
22. ACD/Percepta, 2012 Build 2203, Advanced Chemistry Development, Inc., Toronto, On, Canada, http://www.acdlabs.com.
23. Giannetti, A. M.; Zheng, X.; Skelton, N. J.; Wang, W.; Bravo, B. J.; Bair, K. W.; Baumeister, T.; Cheng, E.; Crocker, L.; Feng, Y.; Gunzner-Toste, J.; Ho, Y.-C.; Hua, R.; Liederer, B. M.; Liu, Y.; Ma, X.; O'Brien, T.; Oeh, J.; Sampath, D.; Shen, Y.; Wang, C.; Wang, L.; Wu, H.; Xiao, Y.; Yuen, P.; Zak, M.; Zhao, G.; Zhao, Q.; Dragovich, P. S. *J. Med. Chem.* **2014**, *57*, 770.
24. Zheng, X.; Bauer, P.; Baumeister, T.; Buckmelter, A. J.; Caligiuri, M.; Clodfelter, K. H.; Han, B.; Ho, Y.-C.; Kley, N.; Lin, J.; Reynolds, D. J.; Sharma, G.; Smith, C. C.; Wang, Z.; Dragovich, P. S.; Gunzner-Toste, J.; Liederer, B. M.; Ly, J.; O'Brien, T.; Oh, A.; Wang, L.; Wang, W.; Xiao, Y.; Zak, M.; Zhao, G.; Yuen, P.; Bair, K. W. *J. Med. Chem.* **2013**, *56*, 6413.